

ENHANCED RED EMISSION OF 1D $\text{CaYAl}_3\text{O}_7: \text{Eu}^{3+}$ PHOSPHOR VIA CO-DOPING Sm^{3+} OR $\text{Li}^+/\text{Na}^+/\text{K}^+$ PREPARED BY ELECTROSPINNING

Q. LI^a, Y. F. ZHANG^{b,*}, Q. LIU^a, Z. L. WANG^b, C. JU^b

^a School of Material Science & Engineering, Qilu University of Technology Shandong Academy of Sciences, Jinan, Shandong, 250353, PR China

^b School of Mechanical & Automotive Engineering, Qilu University of Technology Shandong Academy of Sciences, Jinan, Shandong, 250353, PR China

In this study, a series of one-dimensional $\text{CaYAl}_3\text{O}_7: \text{Eu}^{3+}$ and $\text{CaYAl}_3\text{O}_7: \text{Eu}^{3+}, \text{R}$ ($\text{R} = \text{Sm}^{3+}$ or $\text{Li}^+, \text{K}^+, \text{Na}^+$) phosphors were synthesized by electrospinning. The formation, structure and photoluminescence properties of the phosphors were examined by thermogravimetric differential thermal analysis (TG-DTA), x-ray powder diffraction (XRD), scanning electron microscope (SEM) and photoluminescence spectroscopy (PL). The results show that one-dimensional materials with well crystallization were obtained, and the diffraction peaks of the samples are in good agreement of standard card (JCPDS: 49-0605). The emission spectrum is dominated by a red peak centered at 617 nm due to the $5\text{D}^0 \rightarrow 7\text{F}^2$ transition of Eu^{3+} ions. Concentration quenching occurs when the Eu^{3+} concentration is about 13 mol %, and the critical transfer distance of the phosphor is also calculated. With the increase of the concentration of doped Sm^{3+} ions, the luminescent intensity increased, and reached the maximum at the Sm^{3+} concentration of 10 mol %. The energy transfer processes between Sm^{3+} and Eu^{3+} is investigated in detail. Furthermore, Li^+, Na^+ and K^+ ions were designed as charge compensators to maintain the charge balance of $\text{CaYAl}_3\text{O}_7: \text{Eu}^{3+}$, and the luminescence intensities can be effectively enhanced, especially by Li^+ ion.

(Received August 4, 2020; Accepted November 16, 2020)

Keywords: White LEDs, Red emitting phosphors, Luminescence properties, Electrospinning, Energy transfer

1. Introduction

The fourth generation of lighting source, white light-emitting diodes (LEDs) has unlimited development potential in the field of lighting due to their advantages such as long life, no pollution, small size, high efficiency and low energy consumption^[1-6].

One way to realize white LED^[7-11] is to use ultraviolet light from UV LED chip or UV laser diode to excite blue-emitting, green-emitting and red-emitting phosphors. The red phosphor is an important additive to adjust the color rendering index. However, the red phosphor has many disadvantages, such as low luminous efficiency and poor chemical stability. So, it is urgent to find

* Corresponding author.: zhangyanfei@qlu.edu.cn

and prepare the red phosphor with stable physical and chemical properties and good optical properties.

Rare earth aluminate is a kind of material with stable physical and chemical properties and excellent optical and mechanical properties. It is often used to develop matrix materials such as solid-state lasers, X-ray counters and X-ray scintillators. At the same time, rare earth aluminate can also be used to produce luminescent materials and catalytic materials with excellent properties. Rare earth aluminate luminescent materials have the advantages of corrosion resistance, radiation resistance, high temperature resistance, non-toxicity and non-radiation, and low preparation cost, which makes it possible to achieve industrial production and various applications.

In recent years, there have been many reports on the synthesis of aluminate materials with various morphologies by various methods, such as solid-state reaction^[12], sol-gel synthesis^[13], hydrothermal process^[14], microwave approach^[15] and solution combustion method^[16] etc. These phosphors have excellent fluorescence properties, regular morphology and good dispersion. However, the research mainly focuses on zero-dimensional particles. With the further development of the research, one-dimensional materials have been widely used in basic research and technology application because of their unique electrical and optical properties.

Electrospinning is a simple, convenient and economical technique for preparing one-dimensional materials. At present, many kinds of one-dimensional nano-rods, nano-fibers, nano-tubes and micro-belts with specific luminescent properties have been successfully prepared by electrospinning technology^[17-19].

Therefore, in this work, CaYAl_3O_7 is used as the base material and doped with two kinds of rare earth ions Eu^{3+} and Sm^{3+} . The rare earth aluminate one-dimensional fluorescent materials are prepared by the combination of electrospinning and sol-gel method. The effects of doping concentration of rare earth and alkaline metal dopants, calcination temperature and calcination time on the luminescent properties of the materials were investigated, which provided theoretical basis and experimental basis for better and wider application of the one-dimensional materials.

2. Experimental

2.1. Preparation

A series of $\text{CaYAl}_3\text{O}_7: \text{Eu}^{3+}, \text{Sm}^{3+}$ were prepared by electrospinning method. The raw materials were high-purity europium oxide (Eu_2O_3), Samarium oxide (Sm_2O_3), analytical reagent Calcium nitrate ($\text{Ca}(\text{NO}_3)_2$), Aluminum nitrate ($\text{Al}(\text{NO}_3)_3$), citric acid ($\text{C}_6\text{H}_8\text{O}_7 \cdot \text{H}_2\text{O}$) and nitric acid (HNO_3). And the viscosity of the solution was controlled by the polyvinylpyrrolidone (PVP, $M_w = 1,300,000$).

According to the stoichiometric ratio, the raw materials were weighed accurately with the balance. First Eu_2O_3 , Y_2O_3 and Sm_2O_3 were dissolved in nitric acid solution, then $\text{Ca}(\text{NO}_3)_2$ and $\text{Al}(\text{NO}_3)_3$ were dissolved in deionized water. After all the above substances were dissolved, they were mixed together. Then $\text{C}_6\text{H}_7\text{O}_6$ (citric acid and metal ions 2:1) was added into the mixed solution. In the following, PVP with absolute ethanol was added in the mixed solution was stirred at room temperature for 6 h.

The above solution was added into the syringe with spinneret needle. The positive voltage of 30 kV was added to the anode. The tin plate covered with tin paper was used as collector. The

distance between the needle and the collector was adjusted to 10 cm. Under the action of electric field, the fibers emitted from the spinneret are collected directly on the collector. Finally, the luminescent material was prepared by calcining the collected fibers in crucible at high temperature.

2.2 Materials characterization

The X-ray diffraction (XRD) patterns of the phosphor were obtained on an X Pert PRO MPD diffractometer (PANalytical B.V, Netherlands) operated at 40 KeV and 40 mA with a Cu Ka radiation ($\lambda = 0.15418$ nm) in the range of 10–60°. The morphologies and microstructures of the phosphor were evaluated by scanning electron microscopy (SEM, FEISirion200, Philips, Netherlands). Thermogravimetric analysis (TGA) was performed on a TA TGA equipment (N5350030, Perkin Elmer). The fluorescence properties of the phosphor were investigated by using fluorescence spectrophotometer (RF-5301PC, Shimadzu, Japan). The decay curves were measured at room temperature by FLS920-combined Time Resolved and Steady State Fluorescence Spectrometer (Edinburgh Instruments).

3. Results and discussion

3.1. X-ray diffraction (XRD) analysis

Fig. 1 shows the XRD pattern of $\text{CaYAl}_3\text{O}_7: \text{Eu}^{3+}, \text{Sm}^{3+}$ prepared by electrospinning, as well as the standard card of CaYAl_3O_7 (JCPDS no. 49-0605) as a reference. All the diffraction peaks can be indexed to the tetragonal phase of CaYAl_3O_7 , according to JCPDS no. 49-0605, and no other impurity peaks are found. This indicates that $\text{Eu}^{3+}, \text{Sm}^{3+}$ ions can be efficiently built into the CaYAl_3O_7 host lattice and do not give rise to the change of crystal phase. After annealing at 750 °C (Figure 1b), all the diffraction peaks increase in intensity due to increased crystallinity. At 800 °C, the intensity reaches its maximum, but when the calcination temperature continues to increase, the intensity decreases. This is mainly due to excessive energy absorption and over-sintering and over-growth when calcination temperature is too high.

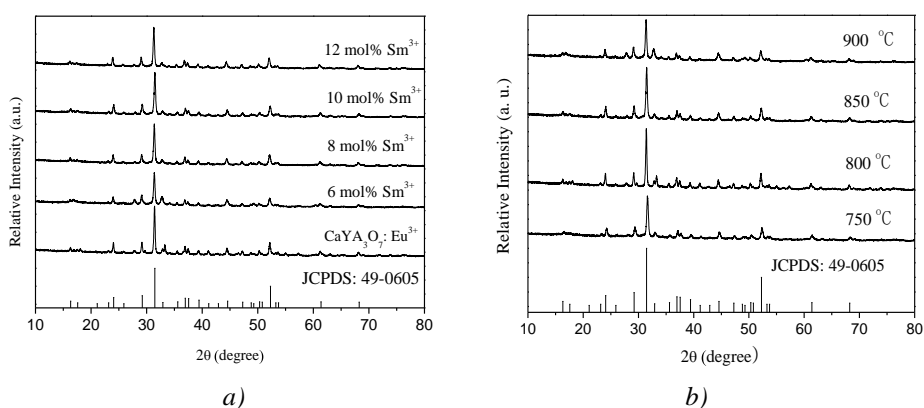


Fig. 1. The XRD spectra of (a) $\text{CaYAl}_3\text{O}_7: \text{Eu}^{3+}, \text{Sm}^{3+}$ phosphor and (b) $\text{CaYAl}_3\text{O}_7: \text{Eu}^{3+}$ at different calcination temperatures.

3.2. TG-DTA

Fig. 2 shows the TG-DTA curves of the as-formed precursor in air. It can be seen from the figure that in the range of room temperature to 130 °C, the TG curve shows that the sample has only slight weightlessness (about 7%) due to the volatilization of absolute ethanol and deionized water. In the range of 130 °C-150 °C, the TG curve showed a marked decline accompanied by an exothermic peak in the DTA curve. The main reason for weight loss (about 14%) is the thermal decomposition of residual organic matter, citric acid and metal chelates. The weight loss step (about 15%) between 150 and 350 °C accompanied by a strong exothermic peak in the DTA curve may be due to the decomposition of nitrate and polyvinylpyrrolidone branched chain, which escapes in the form of gas. In the range of 350 °C - 500 °C, the weight loss rate is about 37%, which is mainly due to the formation of CO during the decomposition of the main chain of polyvinylpyrrolidone and the exothermic peak appears on the DTA curve. Finally, the weight loss (only 1%) is from 500 °C -700 °C accompanied with a small endothermic peak near 600 °C in the DTA curve mainly due to the absorption of some energy during the formation of the lattice, basically agreeing with the results of XRD.

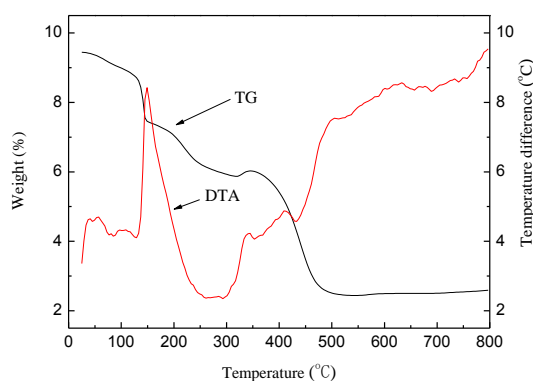


Fig. 2. The TG/DTA curves of $\text{CaYAl}_3\text{O}_7: \text{Eu}^{3+}$ precursor.

3.3. SEM

Fig. 3a and b shows the SEM micrographs of as-formed $\text{CaYAl}_3\text{O}_7: \text{Eu}^{3+}$ precursor and the sample annealed at high temperature (800°C), respectively. From Fig. 3a, it can be seen that these randomly oriented fibers and microbelts have smooth surfaces without adhesion, with a large aspect ratio and about 5~15 μm in diameter. After calcinations at high temperature, a well-defined texture is maintained, as shown in Fig. 3b. It can be seen that after calcining at 800 °C for 5 h, the fibers and belts shrink to a diameter of about 50~150 nm and become rough and curvy. And some of them break. It is mainly due to the evaporation of anhydrous ethanol, the decomposition of PVP and nitrate in the sample after high temperature calcination and the crystallization of $\text{CaYAl}_3\text{O}_7: \text{Eu}^{3+}$.

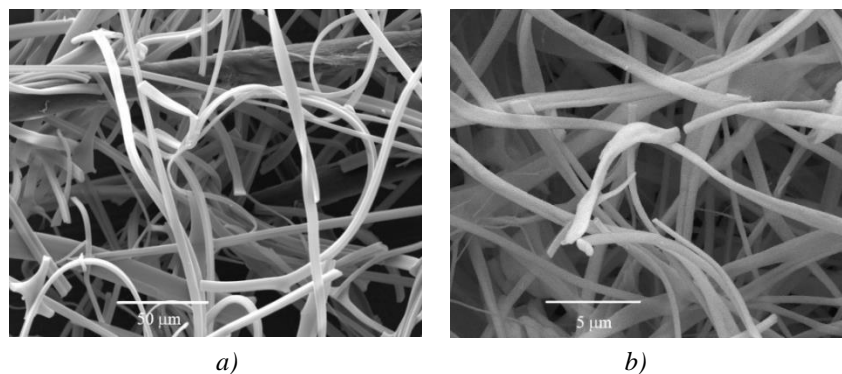


Fig. 3. SEM images of (a) as-formed $\text{CaYAl}_3\text{O}_7: \text{Eu}^{3+}$ precursor and (b) the sample annealed at high temperature (800°C)

3.4. Photoluminescence properties

The PL properties of the as-formed samples were investigated. Figure 4 shows the typical PL excitation (a) and emission (b) spectra of one dimensional $\text{CaYAl}_3\text{O}_7: \text{Eu}^{3+}$.

The excitation spectrum was obtained by monitoring the emission of the $\text{Eu}^{3+} {}^5\text{D}_0 \rightarrow {}^7\text{F}_2$ transition at 617 nm. The excitation spectrum (Fig. 4a) consists of several peaks at 361 nm, 382 nm, 393 nm, 415 nm, and 464 nm, which correspond to ${}^7\text{F}_0 \rightarrow {}^5\text{D}_4$, ${}^7\text{F}_0 \rightarrow {}^7\text{L}_5$, ${}^7\text{F}_0 \rightarrow {}^5\text{L}_6$, ${}^7\text{F}_0 \rightarrow {}^5\text{D}_3$ and ${}^7\text{F}_0 \rightarrow {}^5\text{D}_2$ transition emission of Eu^{3+} ions, respectively. Among them, ${}^7\text{F}_0 \rightarrow {}^5\text{L}_6$ is the strongest excitation band at 393 nm.

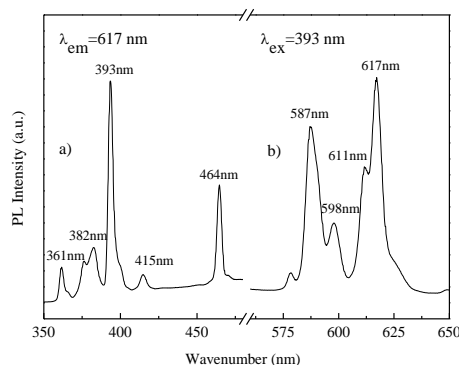


Fig. 4. The excitation a)-emission b) spectra of $\text{CaYAl}_3\text{O}_7: \text{Eu}^{3+}$.

Excitation with 393 nm near-UV light yields an emission spectrum consisting of f-f transitions of Eu^{3+} (Fig. 4b). The dominant red emission bands at 617 nm with a shoulder at 611 nm are attributed to the hypersensitive red-emitting ${}^5\text{D}_0 \rightarrow {}^7\text{F}_2$ transition, indicating that the Eu^{3+} ions locate at the sites of non-inversion symmetry. Other characteristic peaks centered around 587 nm and 598 nm correspond to ${}^5\text{D}_0 \rightarrow {}^7\text{F}_1$ transitions of Eu^{3+} . In addition, we can see that the spectrum exhibits a separated narrow-band emission. This is because when the metastable electrons in Eu^{3+} transit under the shield of 5S5P electron layer, the surrounding electric field will not affect the electrons. Therefore, when the electron cloud is deformed, the energy level of Eu^{3+} will only split into relatively narrow sub-levels. The transition between the energy levels of Eu^{3+}

ions is characterized by magnetic dipole (MD) and electric dipole (ED) transitions. ${}^5D_0 \rightarrow {}^7F_1$ belongs to the magnetic dipole transition of Eu^{3+} ions, which is not affected by outside surroundings. While the ${}^5D_0 \rightarrow {}^7F_2$ belongs to the electric dipole transition of Eu^{3+} ions, which is strongly influenced by outside surroundings and can serve as a very efficient and sensitive structural probe. When the outside surroundings changes, the electric dipole transition especially a transition emission at 617 nm will be greatly affected [20, 21].

The calcination temperature has a certain influence on the luminescent properties of the materials. Fig. 5 shows the emission intensity with different calcination temperature for $\text{CaYAl}_3\text{O}_7:\text{xEu}^{3+}$ ($x = 13 \text{ mol\%}$, 4 h). It can be seen that with the increase of calcination temperature, the luminous intensity of the material first increases and then decreases. When the calcination temperature is 800°C , the luminous intensity of the material reaches the maximum, and when the calcination temperature continues to increase, the luminous intensity of the material decreases. This is mainly due to the over sintering and overgrowth of the materials due to excessive energy absorption when the calcination temperature is too high. From the above analysis, it can be concluded that the synthesis temperature has a great influence on the fluorescence properties of the materials, so in this work, the best calcination temperature is 800°C .

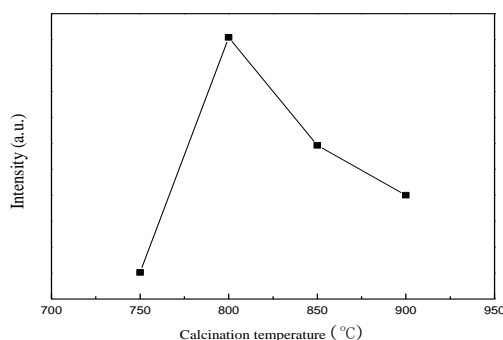


Fig. 5. Emission intensity of $\text{CaYAl}_3\text{O}_7:\text{Eu}^{3+}$ with calcination temperatures.

Fig. 6 plots the emission intensity of the $\text{CaYAl}_3\text{O}_7:\text{xEu}^{3+}$ ($x = 0.07, 0.09, 0.11, 0.13, 0.15$) phosphors versus the Eu^{3+} ion doping concentration. The emission intensity strongly depends on the Eu^{3+} concentration. More specifically, the emission intensity is maximized at an Eu^{3+} concentration of 13 mol% ($x = 0.13$), and reduces at higher and lower concentrations. This trend can be explained by the concentration quenching effect. Initially, with the increase of concentration of Eu^{3+} , the number of active ions entering CaYAl_3O_7 matrix increases and more and more luminescent centers in the matrix results in the increasing luminescent intensity of the material; When the concentration of Eu^{3+} ions exceeds 13 mol%, the distance between Eu^{3+} ions decreases to the critical transfer distance (R_c) which increases the chances of energy transfer and non-radiation transition between Eu^{3+} ions, and consequently consumes part of the energy, resulting in the weakening of the luminescence intensity. Hence the critical transfer distance (R_c) of concentration quenching is calculated by using the relation given by Blasse et al. [22], as per the following:

$$R_c = 2 \times \left(\frac{3V}{4\pi x_c N} \right)^{1/3} \quad (1)$$

where V is the volume of the unit cell, N is the number of host cations in the unit cell, and x_c is the critical concentration of activator (Eu^{3+}).

For the CaYAl_3O_7 host, $N = 2$, $V = 299.66 \text{ \AA}^3$, and X_c is 13% for Eu^{3+} ; Accordingly, the R_c are estimated to be about 6.50 \AA . Exchange interactions and multipolar interactions are the two main reasons for the resonant-type energy-transfer process. It is little possibility of energy transfer through the exchange interaction mechanism with longer distance of more than 5 \AA .^[23] It may be caused by multipole- multipole interaction.

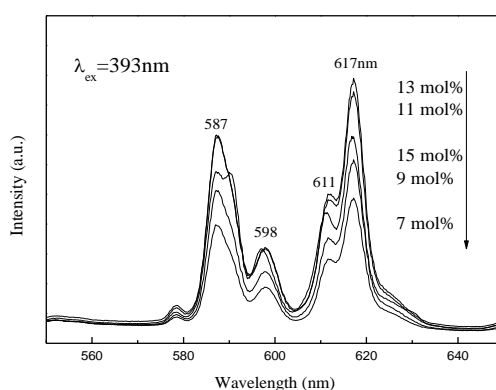


Fig. 6. The emission spectra of $\text{CaYAl}_3\text{O}_7: \text{Eu}^{3+}$ with different Eu^{3+} doping amounts.

Fig. 7 shows the emission spectra of $\text{CaYAl}_3\text{O}_7: 0.13\text{Eu}^{3+}, y\text{Sm}^{3+}$ ($0 \leq y \leq 12 \text{ mol\%}$) phosphors under excitation at 393 nm. The emission spectra consist several characteristic peaks of Eu^{3+} at 587 nm, 598 nm, 611 nm and 617 nm. With the increase of the concentration of doped Sm^{3+} ions, the luminescent intensity first increased and then decreased, and reached the highest at the concentration of 10 mol %, and the position and shape of the emission peak do not change much. When the doping concentration of Sm^{3+} exceeds 10 mol%, the excess Sm^{3+} can aggregate, forming trapping centers that dissipate the absorbed energy instead of transferring it to Eu^{3+} . This energy dissipation reduces the red emissions originating from the ${}^5\text{D}_0 \rightarrow {}^7\text{F}_2$ transition of Eu^{3+} .

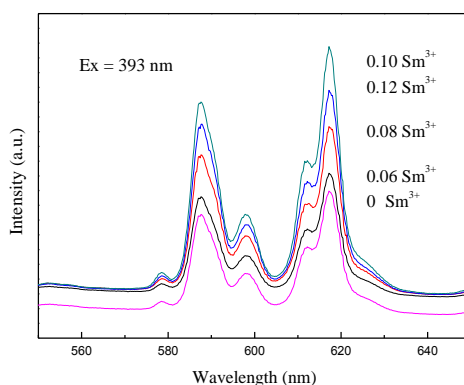


Fig. 7. The emission spectra of $\text{CaYAl}_3\text{O}_7: 0.13\text{Eu}^{3+}, \text{Sm}^{3+}$ with different Sm^{3+} doping amounts.

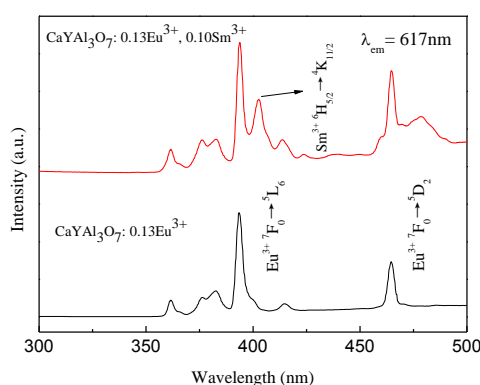


Fig. 8. The excitation spectra of $\text{CaYAl}_3\text{O}_7: 0.13\text{Eu}^{3+}$ and $\text{CaYAl}_3\text{O}_7: 0.13\text{Eu}^{3+}, 0.10\text{Sm}^{3+}$.

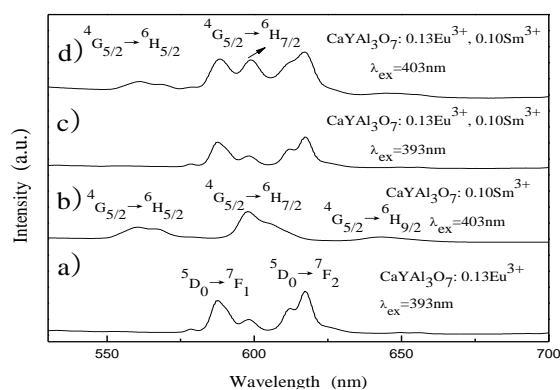


Fig. 9. The emission spectra of $\text{CaYAl}_3\text{O}_7: 0.13\text{Eu}^{3+}$, $\text{CaYAl}_3\text{O}_7: 0.10\text{Sm}^{3+}$ and $\text{CaYAl}_3\text{O}_7: 0.13\text{Eu}^{3+}, 0.10\text{Sm}^{3+}$ excited at different wavelength.

In order to investigate the energy-transfer process from Sm^{3+} to Eu^{3+} in $\text{CaYAl}_3\text{O}_7: \text{Eu}^{3+}, \text{Sm}^{3+}$ samples in more detail, the excitation spectrum of $\text{CaYAl}_3\text{O}_7: 0.13\text{Eu}^{3+}$ and $\text{CaYAl}_3\text{O}_7: 0.13\text{Eu}^{3+}, 0.10\text{Sm}^{3+}$ were obtained by monitoring with 617 nm emission of Eu^{3+} (${}^5\text{D}_0 \rightarrow {}^7\text{F}_2$), as shown in Figure 8. It can be seen that the two strong absorption peaks are located at 393 nm and 466 nm, belonging to the ${}^7\text{F}_0 \rightarrow {}^5\text{L}_6$ and ${}^7\text{F}_0 \rightarrow {}^5\text{D}_2$ transitions of Eu^{3+} respectively. The results show that $\text{CaYAl}_3\text{O}_7: 0.13\text{Eu}^{3+}$ and $\text{CaYAl}_3\text{O}_7: 0.13\text{Eu}^{3+}, 0.10\text{Sm}^{3+}$ luminescent materials can be effectively excited by ultraviolet light at 393 nm and visible light at 466 nm, which indicates that this material can be well matched with ultraviolet light and blue light chips. The excitation spectra of $\text{CaYAl}_3\text{O}_7: 0.13\text{Eu}^{3+}$ doped with Eu^{3+} have strong absorption peaks only at 393 nm in the range of 390–410 nm. When Sm^{3+} ions are introduced, another strong absorption peak appears at 403 nm, corresponding to the ${}^6\text{H}_{5/2} \rightarrow {}^4\text{K}_{11/2}$ characteristic excitation transition of Sm^{3+} . This indicates that energy transfer occurs between Sm^{3+} and Eu^{3+} ions. This will help the phosphor to absorb the light emitted by the near-ultraviolet chip effectively and improve the quantum efficiency.

In addition, a series of emission spectra (excited at 367 nm and 403 nm) of $\text{CaYAl}_3\text{O}_7: 0.13\text{Eu}^{3+}, \text{CaYAl}_3\text{O}_7: 0.10\text{Sm}^{3+}$ and $\text{CaYAl}_3\text{O}_7: 0.13\text{Eu}^{3+}, 0.10\text{Sm}^{3+}$ are shown in Figure 9. In Figure 9a, under excitation at 393 nm, the characteristic emission of Eu^{3+} ions are present

exclusively. The strongest emission peak centered at 617 nm, corresponding to the ${}^5D_0 \rightarrow {}^7F_2$ electric dipole transition of Eu^{3+} red light emission. From Fig. 9b, it can be seen that $\text{CaYAl}_3\text{O}_7:0.10\text{Sm}^{3+}$ samples excited at 403 nm exhibit three characteristic emission peaks, belonging to ${}^4G_{5/2} \rightarrow {}^6H_{5/2}$ (560 nm), ${}^4G_{5/2} \rightarrow {}^6H_{7/2}$ (598 nm) and ${}^4G_{5/2} \rightarrow {}^6H_{9/2}$ (642 nm) of Sm^{3+} ions, respectively. For $\text{CaYAl}_3\text{O}_7:0.13\text{Eu}^{3+}, 0.10\text{Sm}^{3+}$ samples, different excitation wavelengths can produce different emission characteristics. When the material is excited at 393 nm, the emission spectra are consistent with those of Eu^{3+} samples. As shown in Fig. 9c, Sm^{3+} cannot be effectively excited by light at 393 nm, that is, there is no relationship between Eu^{3+} and Sm^{3+} . As shown in Fig. 9d, when the material is stimulated by 403 nm, the characteristic emission peaks of Eu^{3+} are mainly characterized by the characteristic transitions (${}^5D_0 \rightarrow {}^7F_1$ and ${}^5D_0 \rightarrow {}^7F_2$). At the same time, the characteristic emission peaks of Sm^{3+} ions (${}^4G_{5/2} \rightarrow {}^6H_{5/2}$, ${}^4G_{5/2} \rightarrow {}^6H_{7/2}$ and ${}^4G_{5/2} \rightarrow {}^6H_{9/2}$) can be seen, which fully illustrates the energy transfer between Eu^{3+} and Sm^{3+} , which makes the characteristic emission peaks of Eu^{3+} (${}^5D_0 \rightarrow {}^7F_1$ and ${}^5D_0 \rightarrow {}^7F_2$) are present.

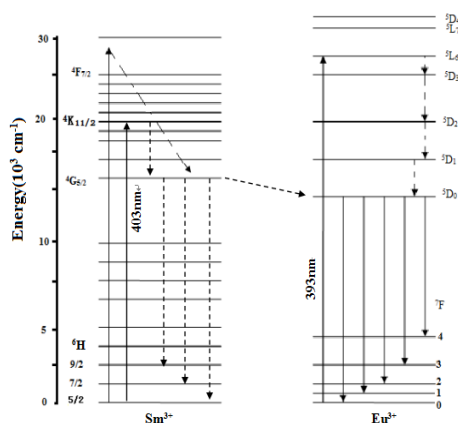


Fig. 10. Excitation, energy transfer, and emission processes of Sm^{3+} and Eu^{3+} in the $\text{CaYAl}_3\text{O}_7: 0.13\text{Eu}^{3+}, 0.10\text{Sm}^{3+}$ phosphor.

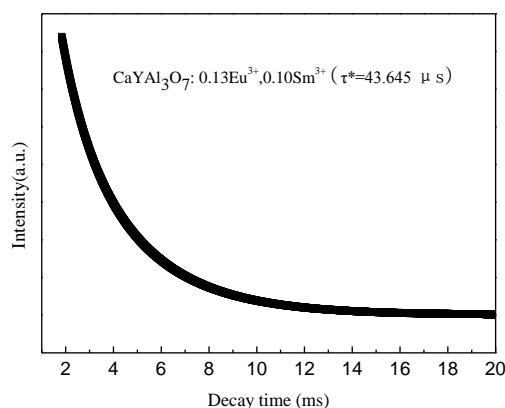


Fig. 11. The decay curves of Eu^{3+} emission for $\text{CaYAl}_3\text{O}_7: 0.13\text{Eu}^{3+}, 0.10\text{Sm}^{3+}$ phosphors ($E_x = 393 \text{ nm}$, $E_m = 617 \text{ nm}$).

Fig. 10 shows a summary of the emission and energy transfer processes in $\text{CaYAl}_3\text{O}_7: 0.13\text{Eu}^{3+}, 0.10\text{Sm}^{3+}$ samples. Under near-ultraviolet light at 403 nm, the electron of sensitizer Sm^{3+} ion is excited the ground state to the excited state $^4\text{K}_{11/2}$. In the excited state, the electron either relaxes to the $^4\text{G}_{5/2}$ level, and then jump back to the ground state from the level of $^4\text{G}_{5/2}$ to produce the red emission or transfer its energy to the level of $^5\text{D}_0$ of Eu^{3+} at this time, which transit back to $^7\text{F}_2$ level and emit 617 nm red emission. Competition between the above two processes results in the occurrence of emission from Eu^{3+} and Sm^{3+} simultaneously in $\text{CaYAl}_3\text{O}_7: 0.13\text{Eu}^{3+}, 0.10\text{Sm}^{3+}$ samples (Fig. 9d).

All the above spectral properties for the $\text{CaYAl}_3\text{O}_7: 0.13\text{Eu}^{3+}, 0.10\text{Sm}^{3+}$ phosphor are basically consistent with the reported bulk, nanocrystalline powder. The decay curve for the representative emission of Eu^{3+} in $\text{CaYAl}_3\text{O}_7: 0.13\text{Eu}^{3+}, 0.10\text{Sm}^{3+}$ was measured, as shown in Fig. 11.

The decay curves can fit well the second-order exponential equation 2

$$I(t) = I_0 + A_1 \exp\left(-\frac{t}{\tau_1}\right) + A_2 \exp\left(-\frac{t}{\tau_2}\right) \quad (2)$$

where $I(t)$ and I_0 are the luminescence intensity at time t and the initial intensity, respectively, A_1 and A_2 are constants, and τ_1 and τ_2 are the decay time values of the exponential components. Additionally, average lifetime (τ^*) are obtained using the A and τ values according to equation 3

$$\tau^* = \frac{(A_1\tau_1^2 + A_2\tau_2^2)}{(\tau_1A_1 + \tau_2A_2)} \quad (3)$$

Table 1. Decay lifetime of Eu^{3+} in $\text{CaYAl}_3\text{O}_7: 0.13\text{Eu}^{3+}, 0.10\text{Sm}^{3+}$ phosphors.

Sample	τ_1	A_1	τ_2	A_2	τ^* (μs)
$\text{CaYAl}_3\text{O}_7: 0.13\text{Eu}^{3+}, 0.10\text{Sm}^{3+}$	2691.95852	33230.0338 1	43.54564	2.4624E22	43.65

The A and τ values calculated from equation 2 are shown in Table 1. The average luminescence lifetimes τ^* of the as-prepared $\text{CaYAl}_3\text{O}_7: 0.13\text{Eu}^{3+}, 0.10\text{Sm}^{3+}$ was 43.65 μs .

3.5. Impact of alkaline metal doping

In the crystal structure of a substance, when cations are replaced by elements of different valence states, there will be internal charge imbalance in the structure. In this paper, alkali metal ions are used to compensate the charge imbalance while doping the activator in order to improve the luminescent intensity of the material.

Fig. 12 shows the emission spectra of $\text{CaYAl}_3\text{O}_7: \text{Eu}^{3+}$ with different charge compensation. The emission spectra of $\text{CaYAl}_3\text{O}_7: \text{Eu}^{3+}$ without charge compensation and Li^+ , Na^+ , K^+ with charge compensation are very similar, but the intensity is different. It can be seen from Fig. 12 that all three charge compensators can significantly improve the luminescent properties of fluorescent materials. It can be clearly seen that the effect of doping Li^+ is the best, because the radius of Li^+ in

alkali metal ions is the smallest, which is more conducive to doping into the lattice; in addition, the introduction of Li^+ can compensate for the charge imbalance caused by oxygen vacancies in materials, reduce the defects of crystal structure itself, so as to improve the transition emission probability of Eu^{3+} and enhance its emission^[24,25]. Thus, the luminescent properties of fluorescent materials can be improved.

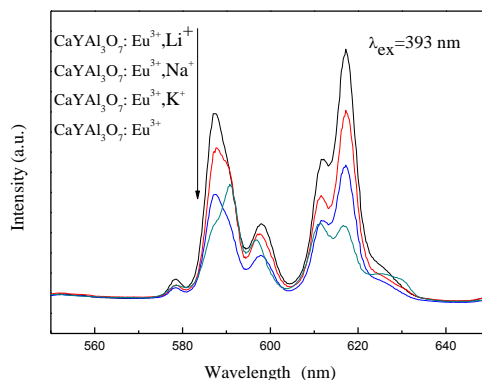


Fig. 12. Emission spectra of $\text{CaYAl}_3\text{O}_7: \text{Eu}^{3+}, M$ ($M = \text{Li}^+, \text{Na}^+, \text{K}^+$).

4. Conclusions

A series of $\text{CaYAl}_3\text{O}_7: \text{Eu}^{3+}, R$ ($R = \text{Sm}^{3+}, \text{Li}^+, \text{K}^+, \text{Na}^+$) red phosphors were synthesized by electrospinning in conjunction with the sol-gel process. The as-formed precursor samples present a smooth surface and uniform fiber or belt morphologies. After being heated at 800°C for 3 h, the as-formed samples are well-crystallized and still maintain their original morphologies, except for the decreasing diameters. Spectral analysis indicated that luminescence intensity in $\text{CaYAl}_3\text{O}_7: \text{Eu}^{3+}$ excited at 393nm is enhanced by co-doping with $\text{Sm}^{3+}/\text{Li}^+, \text{Na}^+,$ and K^+ ions. The prepared phosphors could be efficiently excited under near-ultraviolet light at 393nm and 403 nm. Due to an efficient energy transfer from the Sm^{3+} to Eu^{3+} ions, Eu^{3+} ions show its characteristic strong emissions in the $\text{CaYAl}_3\text{O}_7: \text{Eu}^{3+}, \text{Sm}^{3+}$ 1D nanomaterials upon excitation at 403 nm, corresponding to the ${}^6\text{H}_{5/2} \rightarrow {}^4\text{K}_{11/2}$ characteristic excitation transition of Sm^{3+} .

Acknowledgements

The project was supported by “20 Policies about Colleges in Jinan” Program (Grant NO: 2019GXRC047) and the provincial innovation and entrepreneurship training program of Qilu University of Technology (S202010431089).

References

- [1] H. S. Jang, H. Yang, S. W. Kim et al., *Advanced Materials*, **20**, 2696 (2008).
- [2] Y. X. Gu, Q. H. Zhang, H. Z. Wang et al., *Journal of Materials Chemistry* **21**, 17790 (2011).
- [3] S. Nakamura, *MRS Bulletin* **34**, 101 (2009).
- [4] S. LEE, J. M. SEO, M. LEE et al., *Industrial Crops and Products* **54**, 320 (2014).
- [5] Y. Kim, P. Arunkumar, B. Y. Kim et al., *Nature Materials* **16**, 543 (2017).
- [6] P. Pust, P. J. Schmidt, W. Schnick, *Nature Materials* **14**, 454 (2015).
- [7] X. M. Han, X. Yan, J. Q. Qi et al., *Journal of Nanoscience and Nanotechnology* **16**, 730 (2016).
- [8] Z. G. Lei, X. L. Zhang, D. Wang et al., *Journal of Materials Science-Materials in Electronics* **27**, 7089 (2016).
- [9] R. P. Cao, Z. D. Qin, S. H. Jiang et al., *Bulletin of Materials Science* **39**, 187 (2016).
- [10] B. Wang, H. Lin, F. Huang et al., *Chemistry of Materials* **28**, 3515 (2016).
- [11] X. Zhang, J. Wang, L. Huang et al., *ACS Applied Materials & Interfaces* **7**, 10044 (2015).
- [12] P. Upadhyay, D. Verma, A. Bourase et al., *Int. J. Lumin. Appl.* **5**, 239 (2015).
- [13] R. Y. Zhang, A. Khalizov, L. Wang et al., *Chemical Reviews* **112**, 1957 (2012).
- [14] X. Li, H. Pan, A.W. Tang et al., *Journal of Nanoscience and Nanotechnology* **16**, 3474 (2016).
- [15] Y. Zhang, J. Xu, Q. Cui, et al. *Scientific Reports* **7**, 42464 (2017).
- [16] W. B. Lu, M. Zu, J. H. Byun et al., *Advanced Materials* **24**, 1805 (2012).
- [17] L. L. Wang, Z. Y. Hou, Z. W. Quan et al., *Inorganic Chemistry* **48**, 6731 (2009).
- [18] Z. Hou, C. X. Li, J. Yang et al., *Journal of Materials Chemistry* **19**, 2737 (2009).
- [19] Li, Z. Hou, C. Peng et al., *Advanced Functional Materials* **20**, 3446 (2010).
- [20] Zhang, Y. Hu, L. Chen et al., *Journal of Luminescence* **142**, 116 (2013).
- [21] Yu, X. H. Xu, P. H. Yang et al., *Materials Research Bulletin* **47**, 117 (2012).
- [22] Blasse, *Physics Letters A* **28**, 444 (1968).
- [23] Chiu, W. Liu, C. Chang et al., *Journal of Materials Chemistry* **20**, 1755 (2010).
- [24] F. Guo, T. Chen, L. Luan et al., *Journal of Physics and Chemistry of Solids* **69**, 1905 (2008).
- [25] Golubocić, S. Nikolić, R. Gajić et al., *Journal of the Serbian Chemical Society* **68**, 1001 (2003).